

PCCP

Accepted Manuscript



This is an *Accepted Manuscript*, which has been through the Royal Society of Chemistry peer review process and has been accepted for publication.

Accepted Manuscripts are published online shortly after acceptance, before technical editing, formatting and proof reading. Using this free service, authors can make their results available to the community, in citable form, before we publish the edited article. We will replace this *Accepted Manuscript* with the edited and formatted *Advance Article* as soon as it is available.

You can find more information about *Accepted Manuscripts* in the [Information for Authors](#).

Please note that technical editing may introduce minor changes to the text and/or graphics, which may alter content. The journal's standard [Terms & Conditions](#) and the [Ethical guidelines](#) still apply. In no event shall the Royal Society of Chemistry be held responsible for any errors or omissions in this *Accepted Manuscript* or any consequences arising from the use of any information it contains.

Facile synthesis of core/shell ZnO/ZnS nanofiber by electrospinning and gas-phase sulfidation for biosensor applications

Anna Baranowska-Korczyk,^{*[a, b]} Kamil Sobczak,^[a] Piotr Dłużewski,^[a] Anna Reszka,^[a] Bogdan J. Kowalski,^[a] Łukasz Kłopotowski,^[a] Danek Elbaum,^[a] and Krzysztof Fronc^[a]

^[a] Dr. A. Baranowska-Korczyk, K. Sobczak, Prof. P. Dłużewski, A. Reszka, Prof. B. J. Kowalski, Dr. Ł. Kłopotowski, Prof. D. Elbaum, Dr. K. Fronc
Institute of Physics
Polish Academy of Sciences
al. Lotników 32/46,
PL-02668 Warsaw, Poland

^[b] Dr. A. Baranowska-Korczyk
Nanobiomedical Centre
Adam Mickiewicz University
ul. Umultowska 85,
PL-61614 Poznań, Poland
E-mail: akorczyk@amu.edu.pl

Abstract:

This study describes a new method of passivizing ZnO nanofiber-based devices with a ZnS layer. This one-step process was carried out in H₂S gas at room temperature, and resulted in the formation of a core/shell ZnO/ZnS nanofibers. The study presents the structural, optical and electrical properties of ZnO/ZnS nanofibers formed by a 2 nm ZnS sphalerite crystal shell covering a 5 nm ZnO wurtzite crystal core. The passivation process prevented free carriers from capture by oxygen molecules and significantly reduced the impact of O₂ on nanostructures conductivity. The conductivity of the nanofibers was increased by three orders of magnitude after the sulfidation, the photoresponse time was reduced from 1500 s to 30 s, and the cathodoluminescence intensity increased with the sulfidation time thanks to the removal of ZnO surface defects by passivation. The ZnO/ZnS nanofibers were stable in water for over 30 days, and in phosphate buffers of acidic, neutral and alkaline pH for over 3 days. The by-products of the passivation process did not affect the conductivity of the devices. The potential of ZnO/ZnS nanofibers for protein biosensing is demonstrated using biotin and streptavidin as a model system. The presented ZnS shell preparation method can facilitate the construction of future sensors and protects the ZnO surface from dissolving in biological environment.

Introduction

Zinc oxide (ZnO) nanostructures, due to their optical and electrical properties, are ideal systems for the construction of devices such as light emitting diodes,¹ field emitters,² transistors³ or sensors of UV light⁴ and selected gases.⁵⁻⁷ Recently, as a result of the low toxicity of ZnO,⁸ they have attracted considerable interest in biological and medical applications. ZnO nanomaterials have been used in the design of various biodetectors, as well as bio-imaging and drug delivery systems.⁸⁻¹⁰ The fabrication of an effective biosensor based on ZnO, a compound known to have low stability in biological liquids,^{11,12} is a key challenge today, one that requires a method of passivizing the surface of organic compounds insoluble in water or other low-toxic semiconductor material.

As zinc sulfide (ZnS) has a high chemical stability in alkaline and weakly acidic environments, a layer of ZnS can protect the surface of an object made of ZnO from dissolving.¹³ As it has relatively low toxicity, ZnS has been used to reduce heavy metal toxicity, preventing the formation of Cd²⁺ on the surface of CdSe and the degradation of water pollutants.¹⁴⁻¹⁷ In recent years, several applications of ZnO/ZnS heterostructure have been described, including nanorods,¹⁸⁻²¹ nanowires,²²⁻²⁵ nanocables²⁶, nanobelts²⁷, nanoribbons²⁸ and nanoparticles.^{29,30} These investigations describe the synthesis of ZnO and ZnS nanostructures of various morphologies and properties.

ZnO/ZnS heterostructures are formed generally by the direct synthesis of both nanomaterials or by the sulfidation of ZnO nanostructures, which is usually performed in liquids, at high temperatures or *via* microwave irradiation.^{18,22,29-32} In the ZnO/ZnS heterojunction, the advantageous properties of both semiconductor nanomaterials are combined. ZnO nanostructures exhibit high intensity photoresponse and high electron mobility. Moreover, Klingshrin reports that ZnO demonstrates high thermal conductivity, significant exciton binding energy (60 meV) and sensitivity to environmental conditions.³³ However, other studies note a long response time and low photocurrent stability due to the presence of oxygen vacancies and interstitial zinc atoms in the crystal lattice.^{34,35} ZnS shows a low photocurrent intensity and stability, but its response time is relatively fast compared to ZnO.³⁶ ZnO-based structures have a wide energy gap of about 3.37 eV or 3.29 eV in the wurtzite and zinc blend form, respectively³⁷, while ZnS exhibits an energy gap of about 3.77 eV in the wurtzite structure and 3.72 eV in its cubic form.^{27,28}

The combination of these two nanomaterials in the form of a type-II heterostructure can represent a base for efficient semiconductor device design. The type-II ZnO/ZnS heterostructure band arrangement induces a migration of holes from ZnO to ZnS and electrons

from ZnS to ZnO. Moreover, the ZnS passivation layer on the surface of ZnO enhances its photoluminescence by the removal of surface defects.²³ The oxygen vacancies are filled by sulfur in the sulfidation process.¹⁹ A ZnS coating enhances photocurrent, with a faster response in ZnO photovoltaic devices.^{25,38} A type-II band alignment of core/shell ZnO/ZnS makes it a stable photocatalyst for light-driven hydrogen generation.^{20,39} The ZnO/ZnS heterostructure shows high sensitivity and quantum efficiency and a short response time to environmental stimuli. Its potential for sensing applications has been demonstrated several times: for example, a high-sensitivity glucose detector has been constructed using enzyme-immobilized ZnO/ZnS core/sheath nanowires.²⁴ A ZnO/ZnS heterostructure has also been used to construct light sensors, especially those working in the range of UV-A radiation (320-400 nm), the main cause of skin cancer.²⁷

The present study presents a facile passivation method of whole devices based on ZnO nanostructures. A ZnS layer was formed on ZnO nanofibers (NF) by treatment of ZnO with hydrogen sulfide (H₂S) in gas phase under ambient conditions, with core/shell ZnO/ZnS nanofibers being synthesized as a result of the passivation process. It provides a detailed physical and chemical characterization of the system, which demonstrated a fast photoresponse time, no influence of oxygen molecules on ZnO conductivity and high stability in a biological environment. A quasi-one-dimensional architecture, a polycrystalline structure and a high surface-to-volume ratio are crucial elements for realizing further applications for ceramic electrospun NFs in electronic nanodevices.

Experimental Section

Fabrication of ZnO NF

ZnO nanofibers were obtained by electrospinning⁴⁰⁻⁴² and calcination. The starting suspension was composed of zinc acetate (C₄H₆O₄Zn×2H₂O, CHEMPUR) and an aqueous solution of poly(vinyl alcohol) (PVA) (M_w = 72 000, POCH). PVA (10 wt %) was prepared in DI water at 60 °C and left for a few days to obtain a homogeneous solution. Following this, 0.25 g of zinc acetate was added to 1.25 g PVA suspension and sonicated for 2 h. The electrospinning process took place with a 0.1 ml/h flow rate and 8 kV electric potential between the needle and the substrate. A metallic frame-shaped collector enabled the production of parallel oriented NFs on the substrates for I-V measurements. After the electrospinning process, the nanostructures were calcined at 500 °C for 4 h in air to obtain ZnO nanofibers.

Construction of I-V measuring devices based on ZnO NF

Two parallel electrodes made of aluminum (90 nm thick) covered with gold/palladium alloy (150 nm thick) were deposited on ZnO NFs collected in a regular sequence. A 0.5 mm space between the two electrodes was. To protect ZnO nanofiber-based devices from biological environment, their surfaces were coated with a dielectric layer, with only the active sensing region remaining uncovered. The ZnO NFs were first protected with 0.3 mm wide copper tape before silicon nitride (SiN) was deposited over the entire surface of the devices. The 70 nm SiN layer was obtained by reactive magnetron sputtering of a silicon target in an argon and nitrogen atmosphere. After this process, the copper tape was removed and an active region with the nanofibers was exposed for further analysis. The I-V measurements were performed using a Keithley 2636A Sourcemeter.

Preparation and characterization of core/shell ZnO/ZnS NF on I-V measuring devices

The devices based on ZnO NFs were placed into a 50 ml hermetic chamber in the presence of 4 ml 20% aqueous solution of $(\text{NH}_4)_2\text{S}$ (Merck). The nanofibers were exposed to ammonium sulfide decomposition products for periods of 10 to 180 min. The ZnS shell was synthesized on the ZnO surface as a result of the sulfidation process.

The structural characterization of ZnO/ZnS NF was performed by Transmission Electron Microscopy (TEM) and Energy-Filtered Transmission Electron Microscopy (EFTEM) analysis (JEM2000EX and TITAN CUBED 80-300). The chemical composition was investigated by Energy Dispersive X-ray Spectroscopy (EDX, TITAN CUBED 80-300). The substrates of the samples used for TEM, EFTEM and EDX measurements were in the form of square 300-mesh gold grids. The optical properties of ZnO/ZnS nanofibers were probed by cathodoluminescence (CL) (Gatan MonoCL-3) with an incident beam current 6.46 nA and accelerating voltage of 15 keV at room temperature. The electrospun nanofibers for CL analysis were deposited on silicon substrates and then calcined at 500 and 700 °C for 4 h. The photoresponses of ZnO and ZnO/ZnS NF were revealed by illuminating the sample with a He-Cd laser (325 nm, 200 mW/cm²). The applied bias was 10 V.

Stability studies of the ZnO/ZnS nanofibers in water and buffers

The samples were synthesized on 10 x 10 mm Si substrate by electrospinning. Then, they were calcined at 500 °C for 4 h in air to obtain the ZnO nanofibers. After these processes, every sample was cutted in half. One piece of the sample was treated by H₂S and then both of

them was immersed in selected liquids. The ZnO/ZnS and the ZnO (control samples) nanofibers were immersed in DI water (0.08 μ S) for 30 days. In addition, the nanofibers were immersed in 66 mM phosphate buffer (PBS) at different pH values (5.6, 6.8 and 8.0) for 70 hours. The impact of the biological liquids was studied by Scanning Electron Microscopy (SEM, Hitachi SU-70). The NFs were deposited on silicon substrates for SEM analysis.

Preparation of ZnO/ZnS nanofiber-based protein sensor

The ZnO/ZnS nanofibers were functionalized with a 2,2'-bithiophene and biotin complex. The thiophene-biotin conjugate was dissolved in 1,2-dichlorobenzene. The ZnO/ZnS nanofiber area between two electrodes was treated with 5 μ l of the solution for 15 minutes at room temperature. After the incubation process, the sensors were repeatedly rinsed with 1,2-dichlorobenzene. Streptavidin labeled with horseradish peroxidase (HRP), a biotin-binding protein, was selected to analyze the detection processes. A solution of 0.1 mg/ml streptavidin-HRP conjugate in phosphate buffer at pH 7.0 was tested. The detection process was carried out for 5 minutes at ambient conditions. Afterwards, the sensors were also rinsed several times with phosphate buffer to remove excess unbound protein. At each stage of the experiment, I-V characteristics were measured.

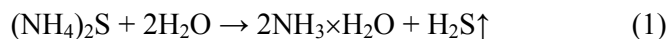
In addition, the HRP enzyme used to label the protein was used for the colorimetric detect of streptavidin *via* the biotin-tiophene complex. In the presence of 2,2'-azino-bis(3-ethylbenzothiazoline-6-sulphonic acid) (ABTS) and hydrogen peroxide (H_2O_2), HRP converts ABTS from a colorless reduced form to colored oxidized one. The reaction was performed on the sensor with 5 μ l of 9 mM ABTS solution in phosphate buffer at pH 5.2 and 0.3 % H_2O_2 . The oxidized form of ABTS was detected using colorimetric and spectrophotometric analysis. The absorption spectra were collected by a Carry 50 Scan spectrophotometer (Varian, USA) at room temperature.

Results and Discussion

In this investigation, the ZnO nanofibers were synthesized by electrospinning followed by calcination in air: a process described in detail in our previous studies.^{40,41} In the first step, the nanofibers were deposited on the substrates to act as a base of the future sensors, which were consecutively calcined at 500 $^{\circ}$ C for 4 h to obtain the ZnO nanostructures (Fig. 1a).

In the next step, two parallel electrodes separated by 0.5 mm were deposited on the NFs (Fig. 1a). The entire ZnO devices were placed in a hermetic chamber (50 ml) in the presence of 20% aqueous ammonium sulfide solution: $(NH_4)_2S$. The NFs were exposed to hydrogen

sulfide (H_2S), the gaseous decomposition product of $(\text{NH}_4)_2\text{S}$, at room temperature. The reaction was carried out for 10, 20, 60 or 180 min. As a result, a thin zinc sulfide layer no thicker than 5 nm was observed on the ZnO surface after 180 min of reaction time (Fig. 1b). The core/shell ZnO/ZnS nanofibers were obtained according to the following reactions (1, 2):



The structural properties of the NFs were studied by TEM. The electron diffraction pattern for a single ZnO/ZnS nanofiber revealed the presence of both hexagonal ZnO (wurtzite) and cubic ZnS (sphalerite) crystal structures in nanofibers treated by H_2S for at least 20 min. Moreover, the Bragg's spots were revealed in the electron diffraction pattern, which indicated that they were polycrystalline (Fig. 2a). Earlier dark-field TEM results⁴⁰ for samples annealed at 500 °C indicated that the mean diameter of the ZnO crystallites amounted to 5 nm. This value is confirmed by the TEM images taken as a part of the present study, which also find the ZnS crystallites to have a diameter of 2 nm (not apparent in Fig. 2b). The high-resolution TEM investigation confirmed the structure of the ZnO crystallite core to be wurtzite and the ZnS shell to be sphalerite. The ZnS shell formation process was investigated for different sulfidation reaction times. The sphalerite coating was found to be present for all selected reaction times, except 10 min: perhaps this time was too short to produce a sufficient concentration of H_2S vapor for its reaction with ZnO to take place. Alternatively, the as-formed shell was not uniform over the entire surface of the NFs and thus remained undetectable by the TEM technique. However, the 20 min sulfidation period was sufficient to form a continuous and homogeneous ZnS coating on the ZnO nanofibers.

The EFTEM analysis of a single ZnO/ZnS nanofiber also confirmed the presence of the ZnS shell (Fig. 3 a-d). Zinc atoms were evenly distributed along the nanofiber, while the amount of oxygen decreased at its edges (Fig. 3 a,b), where the highest content of sulfur atoms was present (Fig. 3c). The superimposition of EFTEM maps for zinc and sulfur atoms revealed a ZnS shell covering the NFs (Fig. 3d).

The atomic composition of the ZnO/ZnS nanofibers was studied by means of EDX (HRTEM). Fig. 4 presents the EDX spectra for the shell and core of the same fiber. The significant differences in intensities of the K line related to sulfur and oxygen indicated that the sulfur concentration was two times higher in the shell than in the central part of NF. However, the signal of oxygen atoms decreased at the edges of the NF.

The optical properties of the ZnO/ZnS NFs were studied by CL measurements. CL spectra were collected from single fibers of the same diameter. Fig. 5 presents the CL spectra for the ZnO nanofibers, annealed at 500 °C for 4h and further treated by H₂S for 10, 15, 20, 60 or 180 minutes. The emission band, centered around 390 nm, is related to band-to-band recombination.³⁷ The intensity of the gap-band emission was found to be higher for the ZnO/ZnS nanofiber than the ZnO (Fig. 5 inset), with the intensity of the CL increasing with the sulfidation process time, indicating the emission mechanisms for NFs coated with ZnS layer were enhanced. Consequently, it can be concluded that the ZnS layer passivated non-radiative defects in ZnO.

To elucidate the mechanism by which the ZnO surface defects were removed, the optical properties of ZnO nanofibers calcined at 700 °C were examined before and after the 20-minute sulfidation process (Fig. 6). Our previous study found the strongest defect emission to be present in NFs calcined at 700 °C, as at this temperature, the surface recombination and generation of oxygen molecules causes the highest concentration of oxygen vacancies. The spectrum for ZnO NF obtained at 700 °C demonstrated two clearly-resolved emission bands (Fig. 6 inset). One, a band-to-band emission, was detected around 390 nm and the other one, at around 520 nm, was a defect band resulting from oxygen vacancies. The intensities of both bands were comparable. After the surface passivation of ZnO by ZnS, the defect band completely disappeared, and the intensity of the band-gap emission increased by several orders of magnitude, indicating the effective passivation of surface defects in ZnO by the ZnS layer.

Core/shell ZnO/ZnS nanofiber-based devices were constructed in the following way. At first, current-voltage sensors based on ZnO nanofibers were prepared and used for various gases and UV radiation detection.⁴⁰ A 70 nm SiN layer was then formed over the entire sidewall surface of the devices, with the exception of the active sensing region with the nanofibers. This dielectric layer prevented the tested liquid influencing the electrical conductivity of the electrodes. Finally, the devices were treated with hydrogen sulfide for 60 min for future ZnO/ZnS biosensors formation, this being sufficient time to form a continuous ZnS shell without excess by-products which require rinsing in water, as would be necessary after 3-hour treatment. The quantity of by-products formed by the process was not significant and did not impede the correct functioning of the devices thus produced.

Fig. 5a shows the current-voltage (I-V) characteristics of the same nanostructures before and after sulfidation. The conductivity of ZnO/ZnS nanofibers was found to be 3.5×10^3 times higher than ZnO NFs. The electrical conductivity of ZnO nanostructures depends on the

adsorption of oxygen molecules on the surface. Due to the capture of O_2 by free carriers, the depleted area of the surface decreases and the conductivity of the nanostructures is reduced.^{40,42} This mechanism presumably was not active at the ZnO passivated surface due to the removal of oxygen surface defects and blockage of the reaction with oxygen molecules, indicating that the ZnS layer prevented the free carriers in ZnO from being trapped by oxygen molecules (Fig. 5a).

Test samples of the substrate without nanofibers were prepared and subsequently treated with H_2S to act as controls for the influence of passivation on the future devices, especially their impact on conductivity. The I-V analysis revealed that both passivated and non-passivated samples were non-conductive (Fig. 5b), and that neither the sulfidation process nor the decomposition products of $(NH_4)_2S$ affect the conductivity of the nanosystems.

Additionally, the ZnO and the core/shell ZnO/ZnS nanofibers were exposed to UV illumination (325 nm, 200 mW/cm²). The conductivity of the ZnO NFs without the ZnS shell increased by three orders of magnitude after 10 s exposure to UV light (Fig. 6a)⁴⁰. This increase in conductivity was related to desorption of oxygen molecules from the ZnO surface. The charge carriers (electrons) trapped in the O_2^- complexes at the surface were released by desorption of oxygen molecules from the surface as a consequence of their activation by UV light. The abundance of excited carriers led to a dramatic increase in conductivity. The photoresponse of the ZnO NFs covered with the ZnS shells was observed to be lower than that of the exposed ZnO nanofibers, this difference being a matter of a few tens of nA (Fig. 6b). However, after switching off the light, the current dropped back to the initial value. The decay time was about 1500 s and 30 s for the ZnO and the ZnO/ZnS nanofibers, respectively (Fig. 6a,b). This slower time associated with the non-passivated nanostructures was dependent on the mechanism associated with the re-adsorption of oxygen molecules on the surface which had been previously illuminated by UV light. The relatively fast decay time observed for the passivated nanostructures confirmed that the ZnS shell was continuous along the ZnO nanofibers and O_2 had no effect on the electrical conductivity.

To study the impact of the biological environment on the ZnO/ZnS nanofibers, the nanostructures were treated with water and various buffers (Fig. 7). Figures 7a and 7b show SEM images of the untreated ZnO and ZnO/ZnS nanofibers, respectively. The passivated and non-passivated nanofibers were immersed in water for 30 days. At the end of this period, the ZnO nanofibers were completely dissolved (Fig. 7c), while ZnO/ZnS nanofibers remained whole (Fig. 7d). The ZnO and ZnO/ZnS nanofibers treated with acidic (pH 5.6), neutral (pH 6.8) or alkaline (pH 8.0) phosphate buffer solution at a concentration of 66 mM, which is

several times higher than the physiological concentration, for 70 h. The SEM images of the ZnO and ZnO/ZnS nanofibers after immersion in the three different pH solutions are given in Figures 7 e-j. Again, the ZnO NFs were dissolved completely for all phosphate buffers (Fig. 7 e,g,i) while the ZnO/ZnS nanofibers remained whole (Fig. 7 f,h,j). These results coincide with Zhou report, in which ZnO 1D nanostructures can remain stable in the fluid only for a few hours before degradation into mineral ions.¹² ZnO nanowires are etched by water, ammonia or NaOH solutions to soluble Zn_2^+ , $\text{Zn}(\text{NH}_3)_4^{2+}$ and ZnO_2^{2-} ions, respectively. The ZnO surface polarity is the major reason of the reaction with phosphate buffers and the etching process.¹¹ ZnO nanocrystals show two interpenetrating sublattices of corner-sharing tetrahedra with Zn^{2+} and O_2^- ions, which form positively charged Zn terminated (0001) and negatively charged O terminated (000-1) faces. Consequently, they can easily interact with both positive and negative charges, such as H_3O^+ or OH^- . Moreover, the etching process is faster for nanomaterials with defects and polycrystalline nanostructures in comparison with the bulk.⁴³ It can be seen that ZnO nanofibers coated with ZnS are insoluble in biological fluids and thus constitute a perfect nanomaterial for future biosensors. In contrast to ZnO-based biosensors, the core/shell ZnO/ZnS nanofibers, no conductivity change was associated with the dissolution. The presence of sulfur can improve the process of further biofunctionalization and immobilize molecules with a thiol groups on the ZnS surface *via* disulfide bonds.

To prepare and study a selective biosensor based on the ZnO/ZnS nanofibers, biofunctionalization and protein detection processes were carried out. Firstly, the nanofibers were functionalized with biotin. The ZnO/ZnS-biotin interaction was realized by the immobilization of a sulfur-containing complex of thiophene and biotin to the ZnS surface (see supplementary information – Fig. 10). The conjugate is attached to the ZnS surface *via* disulfide bonds, which is made possible by the thiol groups of the thiophene, resulting the wrapping of the ZnO/ZnS nanofibers by biotin molecules. The nanostructures were biofunctionalized by biotin for further detection of streptavidin, which has an extraordinarily high affinity (affinity constant $> 10^{15} \text{ M}^{-1}$) for biotin. Hence, the ZnO/ZnS-streptavidin interaction was performed in two steps: biotinylation of ZnS surface using a thiophene-biotin complex following the covalently attachment of streptavidin to biotin. Biotin-streptavidin interaction acted as a model system to allow the working mechanisms of the protein biosensor to be studied in detail.

The sulfuration of ZnO NFs, further biotinylation of the sensor and protein detection resulted in changes in electrical conductivity (Fig. 10). The conductivity of the ZnO/ZnS NFs was greater than that of the untreated nanostructures (Fig. 10 a,b). The biofunctionalization

process decreased the conductivity of the ZnO/ZnS nanofibers (Fig. 10 c), which fell further following the streptavidin detection process (Fig. 10 d). The current-voltage changes related to the biofunctionalization and detection processes are related to the electrical charge of the immobilized biomolecules. The net surface charge depends on the pH of the liquid in which the substance is submerged. The molecules in solution at pH values below the isoelectric point (pI), i.e. the value of pH at which the number of positive and negative charges is equal, and a molecule carries no net electrical charge, gain protons (H^+) and become positively charged, while those pH above pI become negatively charged. As biotin has an ionic equilibrium at pH 4.5,⁴⁴ the molecule was negatively charged in a phosphate buffer at pH 7. The ionization of biotin causes the accumulation of positive charges in the conductive channel (NFs) as a result of the accumulation of negative charge on the ZnO/ZnS surface, leading to a decrease in the conductivity of n-type ZnO NFs. This process is analogical to the basic conduction mechanism in the n-channel MOSFET (Metal-Oxide Semiconductor Field-Effect Transistor), when the gate is negatively polarized to the source. After protein detection, the conductivity decreases again because of the negative charge of the streptavidin-HRP conjugate in the experimental solution (pH 7). A theoretical pI value of 6.24 was calculated for the streptavidin⁴⁵ and horseradish peroxidase⁴⁶ complex using ProtParamsoftware.⁴⁷

The biofunctionalization and protein detection processes were verified by colorimetric techniques by HRP enzyme labeling. HRP catalyzes the conversion of the colorless form of ABTS to green oxidized ABTS in the presence of hydrogen peroxide. After protein binds to the NFs, the reaction with ABTS took place on the sensor. The oxidized form of ABTS was found to have an absorption peak with a maximum at 405 nm. A 20 μ l drop of the reaction products from the sensor was transferred with 1 ml of reaction substrates (ABTS with H_2O_2) to cuvettes for UV/VIS measurements. A 5 μ l amount of streptavidin and HRP of the same concentration used in the reaction on the sensor was used as control. The results are presented in Figure 11. The resulting spectra revealed an absorption peak at 405 nm, indicating that the oxidized form of ABTS was present in both solutions. The intensity of the ABTS peak was significantly reduced after the reaction on the device as the signals originated only from the streptavidin-HRP complex bound to the NFs. As the spectra for ABTS and ABTS with H_2O_2 solutions did not reveal the presence of the oxidized form, the biofunctionalization and detection processes had been performed correctly (Fig. 11 e-g).

The ABTS/ H_2O_2 solution not treated with HRP remained in reduced form and did not change color (Fig. 11e) while the reaction solution changed from colorless to green. The green color of the drop taken from the sensor (Fig. 11 g) was less intense than the color obtained in the

control reaction (Fig. 11 f), despite the fact that the same concentration of protein conjugate and all reactants were applied. This would imply that only part of the proteins was attached to the sensor because the reaction was limited by the biotin concentration on the ZnO/ZnS NFs. The biotin-streptavidin coupling approach was selected to demonstrate the sensing properties of electrospun ceramic nanofibers. The conductivity changes after streptavidin detection and control reactions with HRP enzyme indicate that ZnO/ZnS nanofibers are sensitive and specific protein detector.

Conclusions

The surface passivation technique presented in this report was applied to single nanostructures commonly used in conventional methods, as well as to whole ZnO devices. The by-products of the ZnS coating on ZnO nanofibers do not affect conductivity. The structural characterization of the ZnO/ZnS nanofibers revealed a ZnS shell consisting of 2 nm sphalerite crystals surrounding a ZnO core of 5 nm wurtzite crystals. The conductivity of the nanofibers increases by three orders of magnitude after synthesis of the ZnS shell due to the passivation process inhibiting the effect of oxygen molecules, which capture free carriers from the ZnO nanostructures. For the same reason, no significant increase in conductivity was observed upon UV irradiation and the photoresponse time was reduced from 1500 s to 30 s. The CL intensity of band gap emission of ZnO nanofibers increases with the sulfidation time, while defect emission is inhibited by surface defect passivation. Synthesis of a ZnS shell on a ZnO core is an effective method of protecting ZnO nanostructures against the influence of biological environment. Core/shell ZnO/ZnS nanofibers are stable in water for over 30 days and in high ionic strength phosphate buffers, from acidic to alkaline pH, for over 3 days. This method of laying a ZnS shell on a ZnO nanofibers-based device may be useful in the construction of various biosensors. The ZnO/ZnS nanofibers were used to construct a protein sensor based on as biotin-streptavidin reaction. Our findings indicate that the core/shell ZnO/ZnS nanostructure represents a very promising building block for the fabrication of effective nanodevices in the near future.

Acknowledgements

The research was supported by the European Union as a part of the European Regional Development Fund, through the Innovative Economy (POIG.01.01.02-00-008/08) grant. A. B-K acknowledges financial assistance from National Science Centre (Grant - UMO-2013/11/D/ST5/02900), Nation Centre for Research and Development (Grant - PBS1/A9/13/2012) and the European Social Fund (POKL.04.03.00-00-015/12). The authors

also thank Prof. Włodzimierz Kutner, from the Institute of Physical Chemistry of the Polish Academy of Sciences in Warsaw (IChF PAN) for providing the tiophene-biotin complex samples.

Keywords: ZnO • ZnO/ZnS heterostructure • type-II heterostructure • electrospinning • ZnO devices

- 1 X. Mo, G. Fang, H. Long, S. Li, H. Wang, Z. Chen, H. Huang, W. Zeng, Y. Zhang and C. Pan, *Phys. Chem. Chem. Phys.*, 2014, **16**, 9302-9308.
- 2 J. Song, S. A. Kulinich, J. Yan, Z. Li, J. He, C. Kan and H. Zeng, *Adv. Mater.*, 2013, **25**, 5750-5755.
- 3 Y. C. Shen, C. H. Yang, S. W. Chen, S. H. Wu, T. L. Yang and J. J. Huang, *Biosens. Bioelectron.*, 2014, **54**, 306-310.
- 4 M. R. Alenezi, A. S. Alshammari, T. H. Alzanki, P. Jarowski, S. J. Henley and S. R. P. Silva, *Langmuir*, 2014, **30**, 3913-3921.
- 5 Y. Zhao, X. Lai, P. Deng, Y. Nie, Y. Zhang, L. Xing and X. Xue, *Nanotechnology*, 2014, **25**, 115502.
- 6 N. L. Tarwal, A. R. Patil, N. S. Harale, A. V. Rajgure, S. S. Suryavanshi, W. R. Bae, P. S. Patil, J. H. Kim and J. H. Jang, *J. Alloy Compd.*, 2014, **598**, 282-288.
- 7 P. Zhang and W. Liu, *Biomaterials*, 2010, **31**, 3087-3094.
- 8 W. Wang, Q. Hao, W. Wang, L. Bao, J. Lei, Q. Wang and H. Ju, *Nanoscale*, 2014, **6**, 2710-2717.
- 9 R.-O. Moussodia, L. Balan, Ch. Merlin, Ch. Mustin and R. Schneider, *J. Mater. Chem.*, 2010, **20**, 1147-1155.
- 10 H. M. Xiong, *Adv. Mater.*, 2013, **25**, 5329-5335.
- 11 A. Stafiniak, B. Boratyński, A. Baranowska-Korczyk, K. Fronc, D. Elbaum, R. Paszkiewicz and M. Tłaczała, *Mater. Sci.-Poland*, 2013, **31**, 312-317.
- 12 J. Zhou, N. Xu and Z. L. Wang, *Adv. Mater.*, 2006, **18**, 2432-2435.
- 13 D. Chen, F. Huang, G. Ren, D. Li, M. Zheng, Y. Wang and Z. Lin, *Nanoscale*, 2010, **2**, 2062-2064.
- 14 X. Wang, S. O. Pehkonen and A. K. Ray, *Ind. Eng. Chem. Res.*, 2004, **43**, 1665-1672.
- 15 A. M. Derfus, C. W. Chan and S. N. Bhatia, *Nano Lett.*, 2004, **4**, 11-18.
- 16 K. L. Aillon, Y. Xie, N. El-Gendy, C. J. Berkland and M. L. Forrest, *Adv. Drug Deliv. Rev.*, 2009, **61**, 457-466.

- 17 C. L. Torres-Martinez, R. Kho, O. I. Mian and R. K. Mehra, *J. Colloid Interface Sci.*, 2001, **240**, 525-532.
- 18 Z. Wu, Y. Wu, T. Pei, H. Wang and B. Geng, *Nanoscale*, 2014, **6**, 2738-2745.
- 19 H. X. Sang, X. T. Wang, C. C. Fan and F. Wang, *Int. J. Hydrogen Energy*, 2012, **37**, 1348-1355.
- 20 S. Liu, X. Wang, K. Wang, H. Sang and Z. He, *J. All. Compd.*, 2013, **568**, 84-91.
- 21 S. K. Panda, A. Dev and S. Chaudhuri, *J. Phys. Chem. C*, 2007, **111**, 5039-5043.
- 22 X. Chen, Z. Bai, X. Yan, H. Yuan, G. Zhang, P. Lin, Z. Zhang, Y. Liu and Y. Zhang, *Nanoscale*, 2014, **6**, 4691-4697.
- 23 L. Liu, Y. Chen, T. Guo, Y. Zhu, Y. Su, C. Jia, M. Wei and Y. Cheng, *ACS Appl. Mater. Interfaces*, 2012, **4**, 17-23.
- 24 Y. M. Sung, K. Noh, W. C. Kwak and T. G. Kim, *Sens. Actuators B*, 2012, **161**, 453-459.
- 25 K. Wang, J. J. Chen, Z. M. Zeng, J. Tarr, W. L. Zhou, Y. Zhang, Y. F. Yan, C. S. Jiang, J. Pern and A. Mascarenhas, *Appl. Phys. Lett.*, 2010, **96**, 123105.
- 26 D. Lin, H. Wu, R. Zhang, W. Zhang and W. Pan, *J. Am. Ceram. Soc.*, 2010, **93**, 3384-3389.
- 27 L. Hu, J. Yan, M. Liao, H. Xiang, X. Gong, L. Zhang and X. Fang, *Adv. Mater.*, 2012, **24**, 2305-2309.
- 28 X. Fan, M.-L. Zhang, I. Shafiq, W.-J. Zhang, Ch.-S. Lee and S.-T. Lee, *Adv. Mater.*, 2009, **21**, 2393-2396.
- 29 M. Sookhajian, Y. M. Amin, W. J. Basirun, M. T. Tajabadi and N. Kamarulzaman, *J. Lumin.*, 2014, **145**, 244-252.
- 30 I. Bezverkhyy, J. Skrzypski, O. Safonova and J. P. Bellat, *J. Phys. Chem. C*, 2012, **116**, 14423-14430.
- 31 L. Neveux, D. Chiche, J. Perez-Pellitero, L. Favergeon, A. S. Gay and M. Pijolat, *Phys. Chem. Chem. Phys.*, 2013, **15**, 1532-1545.
- 32 Y. Hu, H. Qian, Y. Liu, G. Du, F. Zhang, L. Wang and X. Hu, *CrystEngComm*, 2011, **13**, 3438-3443.
- 33 C. Klingshirn, *ChemPhysChem*, 2007, **8**, 782-803.
- 34 S. E. Ahn, H. J. Ji, K. Kim, G. T. Kim, Ch. H. Bae, S. M. Park, Y. K. Kim and J. S. Ha, *Appl. Phys. Lett.*, 2007, **90**, 153106.
- 35 K. Liu, M. Sakurai, M. Liao and M. Aono, *J. Phys. Chem. C*, 2010, **114**, 19835-19839.
- 36 X. Fang, Y. Bando, M. Liao, U. K. Gautam, Ch. Zhi, B. Dierre, B. Liu, T. Zhai, T. Sekiguchi, Y. Koide and D. Kolberg, *Adv. Mater.*, 2009, **21**, 2034-2039.

- 37 Ü. Özgür, Ya. I. Alivov, C. Liu, A. Teke, M.A. Reshchikov, S. Doğan, V. Avrutin, S. J. Cho and H. Morkoç, *J. Appl. Phys.*, 2005, **98**, 041301.
- 38 J. Schrier, D. O. Demchenko, L.-W. Wang and A. P. Alivisatos, *Nano Lett.*, 2007, **7**, 2377-2382.
- 39 P. Guo, J. Jiang, S. Shen and L. Guo, *Int. J. Hydrogen Energy*, 2013, **38**, 13097-13103.
- 40 A. Baranowska-Korczyc, K. Fronc, Ł. Kłopotowski, A. Reszka, K. Sobczak, W. Paszkowicz, K. Dybko, P. Dłużewski, B. J. Kowalski and D. Elbaum, *RSC Adv.*, 2013, **3**, 5656-5662.
- 41 A. Baranowska-Korczyc, A. Reszka, K. Sobczak, B. Sikora, P. Dziawa, M. Aleszkiewicz, Ł. Kłopotowski, W. Paszkowicz, P. Dłużewski, B. J. Kowalski, T. A. Kowalewski, M. Sawicki, D. Elbaum and K. Fronc, *J. Sol-Gel Sci. Technol.*, 2012, **61**, 494-500.
- 42 D. Zhang, S. Chava, C. Berven, S. K. Lee, R. Devitt and V. Vatkanant, *Appl. Phys. A*, 2010, **100**, 145-150.
- 43 J. Hüpkes, J. I. Owen, S. E. Pust and E. Bunte, *ChemPhysChem*, 2012, **13**, 66-73.
- 44 H. M. Said, *J. Nutr.* 2009, **139**, 158-162.
- 45 NCBI-CAA00084.1 NCBI Base (The National Center for Biotechnology Information), Protein: Streptavidin [*Streptomyces avidinii*], GenBank: CAA00084.1.
- 46 NCBI-CAA00083.1 NCBI Base (The National Center for Biotechnology Information), Protein: Horseradish peroxidase [*Armoracia rusticana*], GenBank: CAA00083.1.
- 47 E. Gasteiger, C. Hoogland, A. Gattiker, S. Duvaud, M.R. Wilkins, R.D. Appel, A. Bairoch, *Humana Press*, 2005, 571-607.

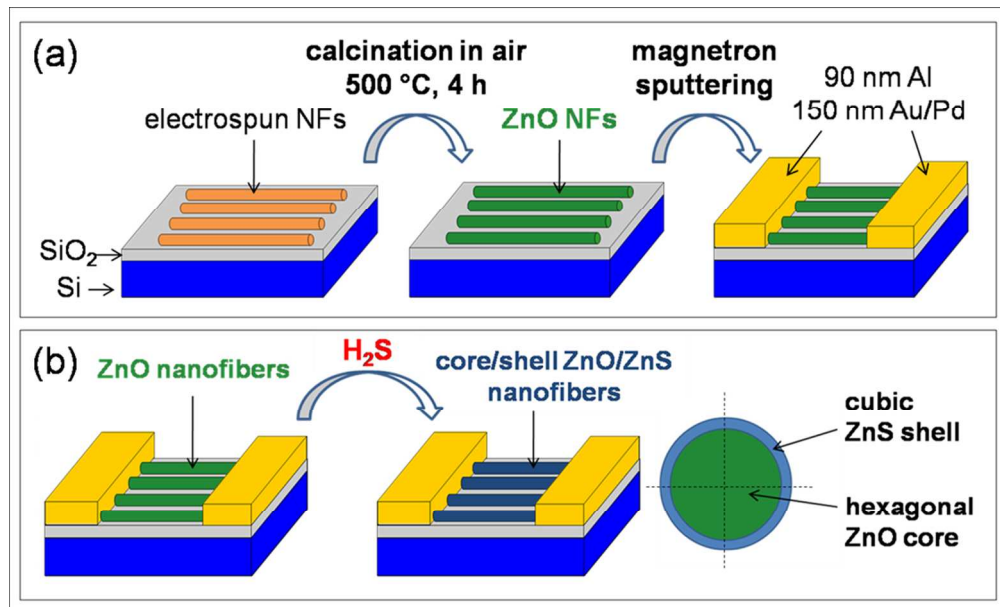


Fig. 1. (a) Schematic diagram of the fabrication of electrospun ZnO nanofiber-based devices. (b) Illustration of the method ZnS surface passivation of ZnO nanodevices.
205x123mm (150 x 150 DPI)

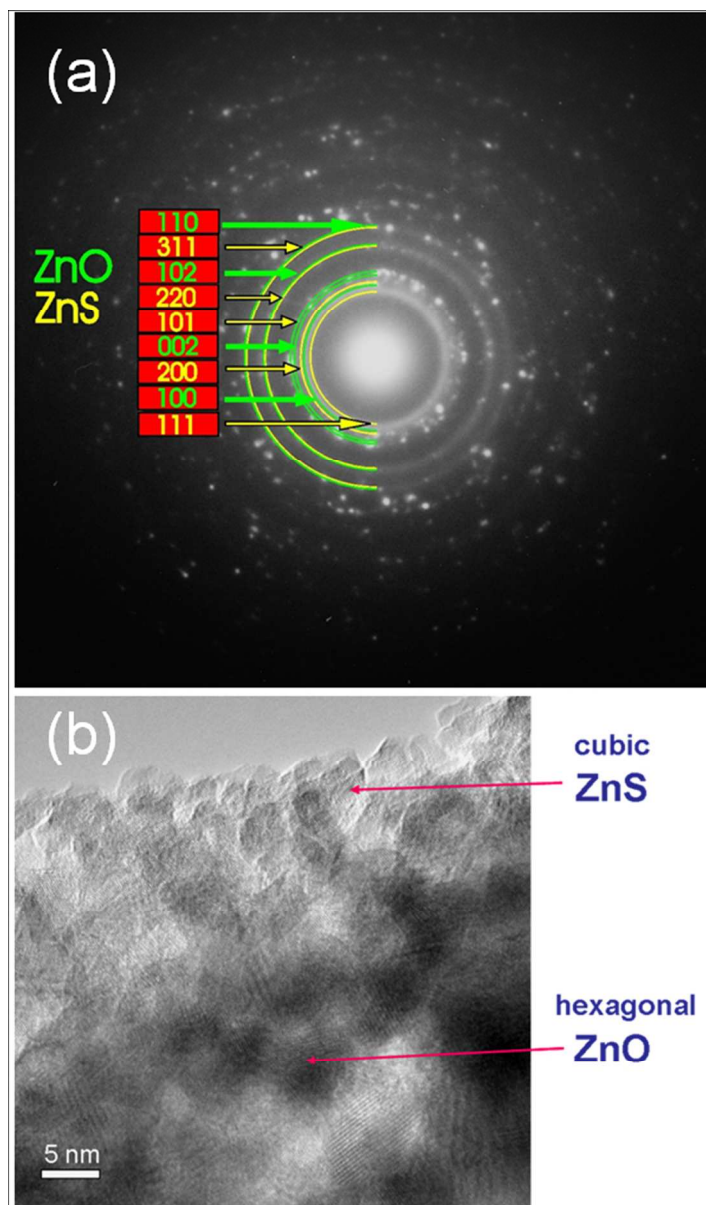


Fig. 2. Electron diffraction pattern (a) and TEM image (b) of ZnO/ZnS nanofiber. The nanostructure was obtained after a sulfidation time of 60 min.
101x172mm (150 x 150 DPI)

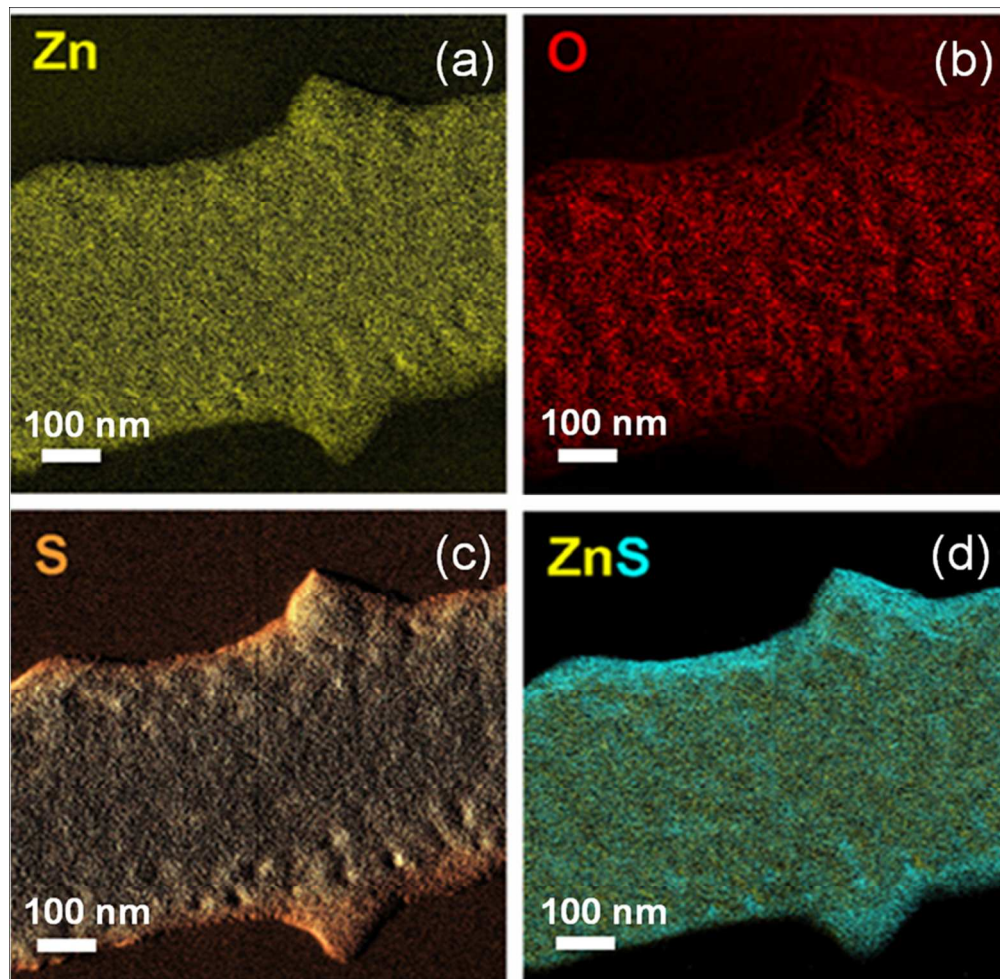


Fig. 3. EFTEM maps of Zn-M (a), O-K (b), S-L (c) and superimposed maps of Zn-M and S-L (d) ZnO/ZnS nanofiber. The nanostructure was obtained after a sulfidation time of 60 min.
189x190mm (141 x 136 DPI)

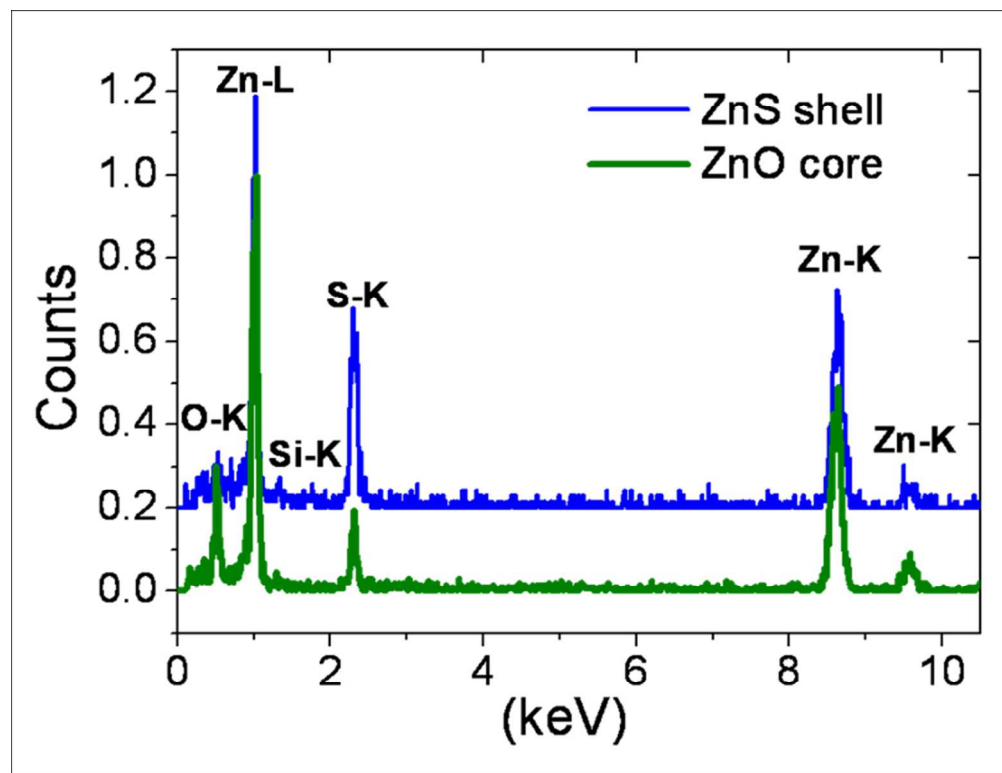


Fig. 4. EDX spectra of the core and shell of the ZnO/ZnS nanofiber. Nanostructure was obtained after a sulfidation time of 60 min.
136x104mm (150 x 150 DPI)

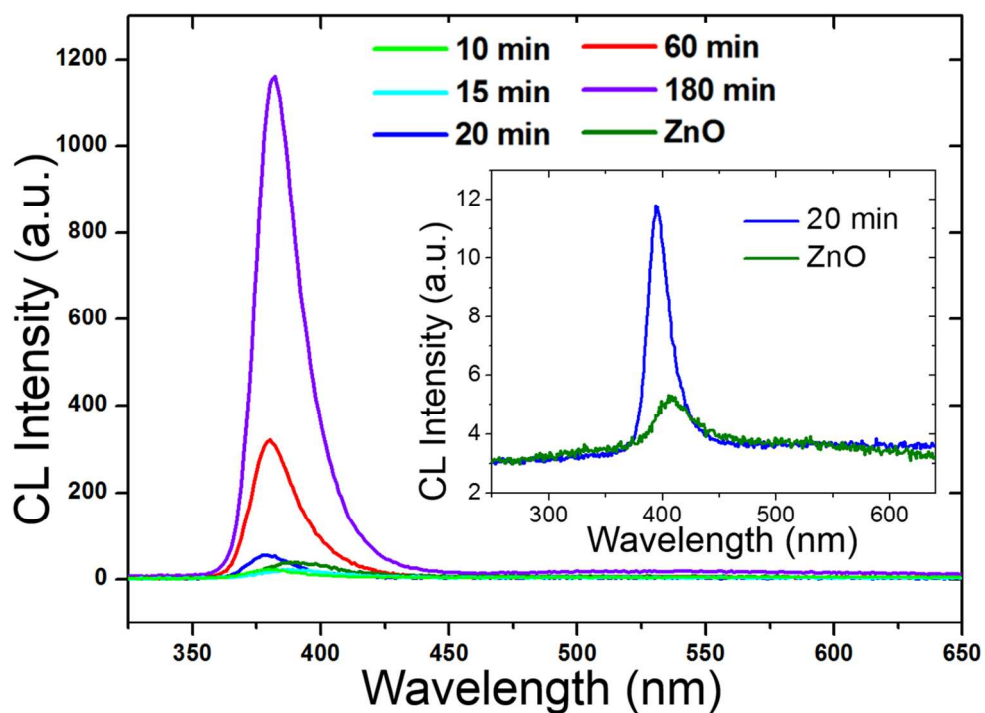


Fig. 5. CL spectra of ZnO and ZnO/ZnS nanofibers. ZnO/ZnS nanostructures were obtained for different sulfidation times, from 10 to 180 minutes. Spectra were collected (with the same magnification) from single fibers of the same diameter ($AV = 15$ KV, $I = 6.46$ nA). The inset is an enlargement of ZnO and selected ZnO/ZnS nanofiber spectra. ZnO/ZnS NF spectrum was obtained for nanostructure after 20 min sulfidation time.

224x164mm (150 x 150 DPI)

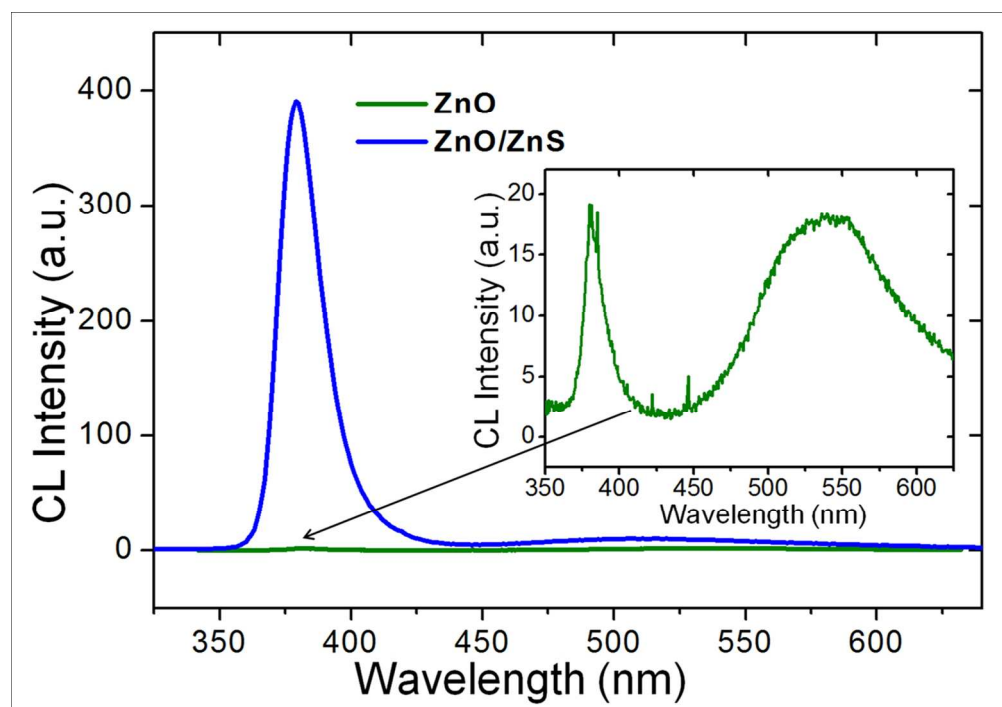


Fig. 6. CL spectra of (a) ZnO nanofiber calcined at 700 °C untreated and (b) treated with hydrogen sulfide for 20 minutes.
254x177mm (150 x 150 DPI)

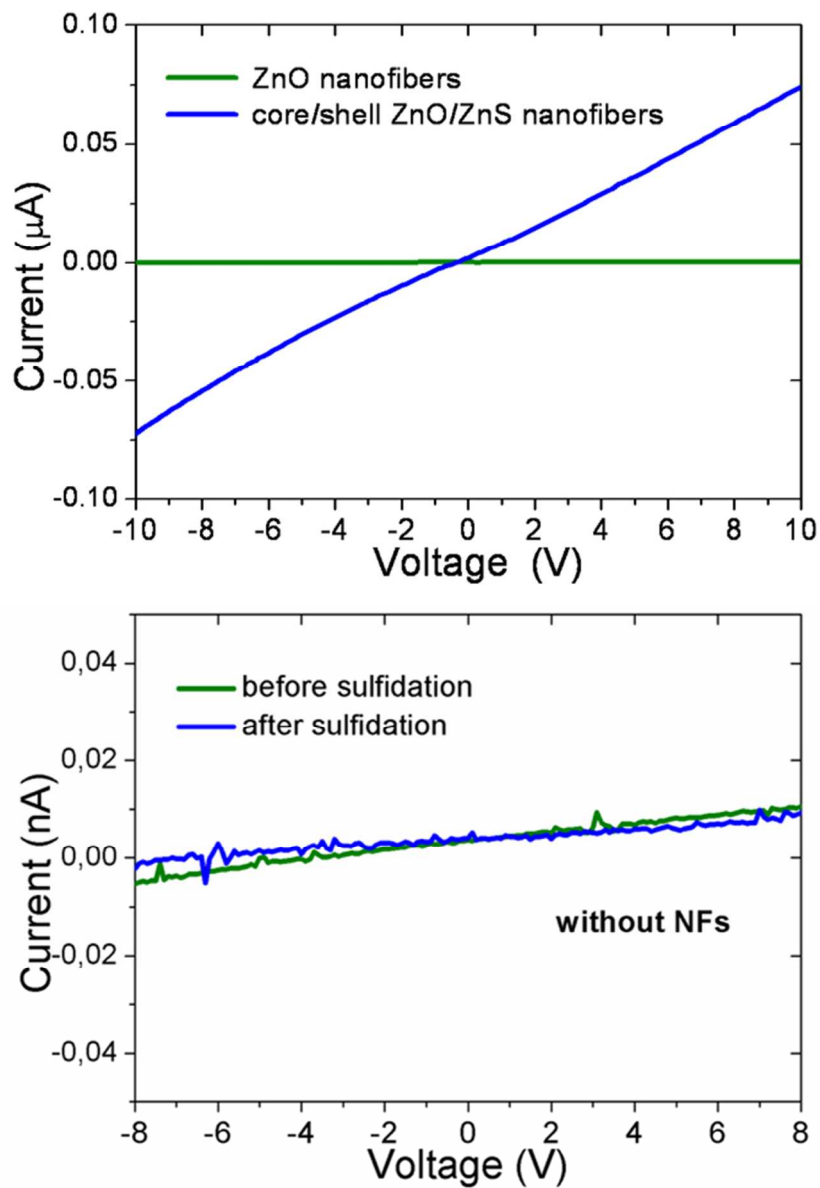


Fig. 7. (a) I-V characteristics of ZnO and ZnO/ZnS nanofibers in air. (b) I-V characteristics of substrate without nanofibers before and after treatment with hydrogen sulfide.
115x165mm (150 x 150 DPI)

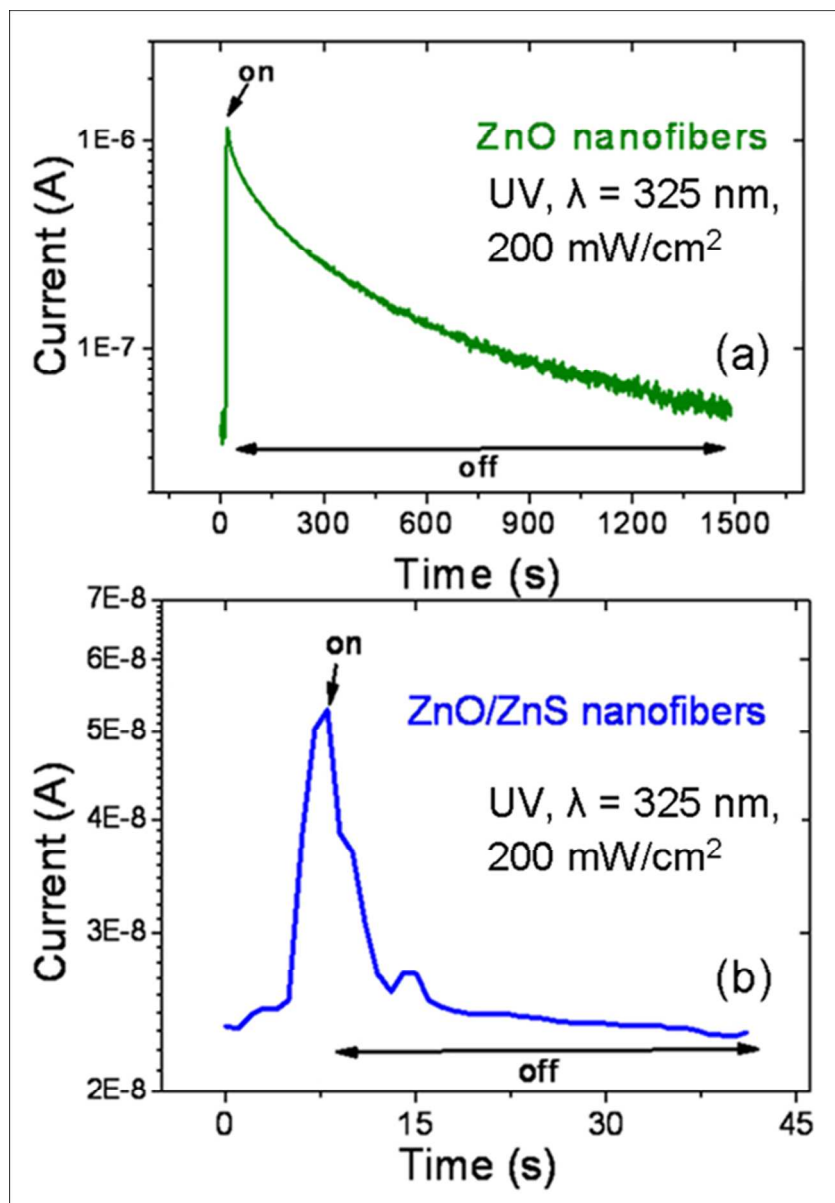


Fig. 8. (a) Photoresponse of ZnO nanofibers with UV light. (b) Photoresponse of core/shell ZnO/ZnS nanofibers with UV light. The bias between two electrodes was 10 V (c,d).
132x190mm (150 x 150 DPI)

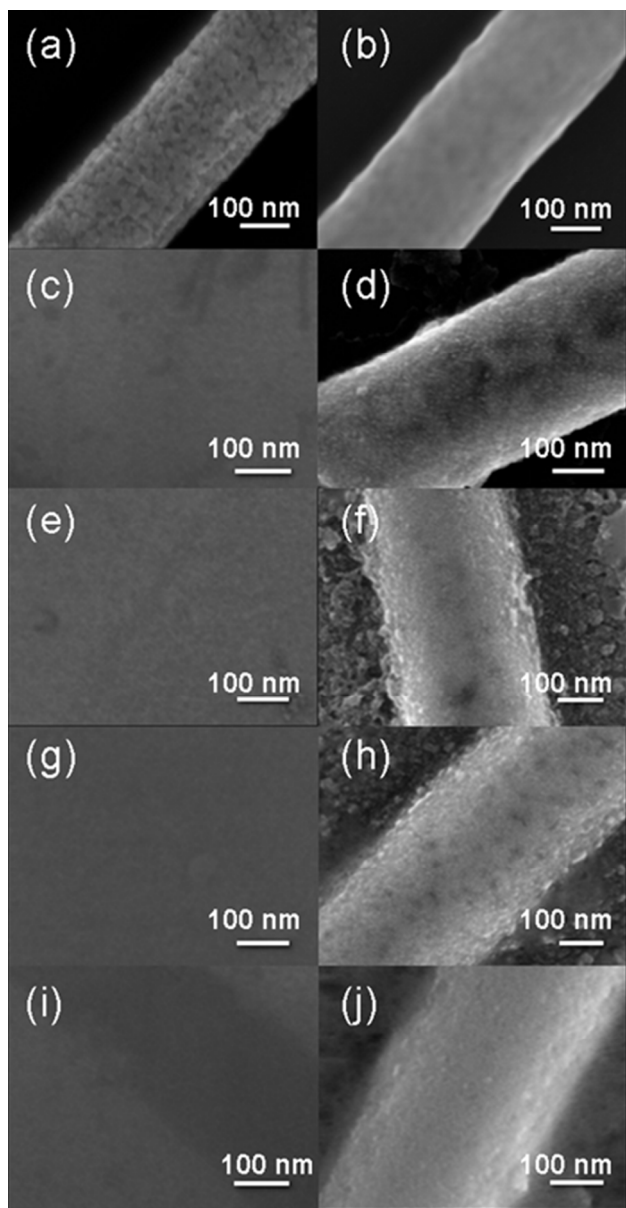


Fig. 9. SEM images of (a),(c),(e),(g) and (i) ZnO and (b),(d),(f),(h) and (j) ZnO/ZnS nanofibers: (a) and (b) untreated with water and buffer; (c) and (d) immersed in water for 30 days; (e) and (f) immersed in 66 mM phosphate buffer at pH 5.6 for 70 h; (g) and (h) immersed in 66 mM phosphate buffer at pH 6.8 for 70 h, (i) and (j) immersed in 66 mM phosphate buffer at pH 8.0 for 70 h.

71x138mm (150 x 150 DPI)

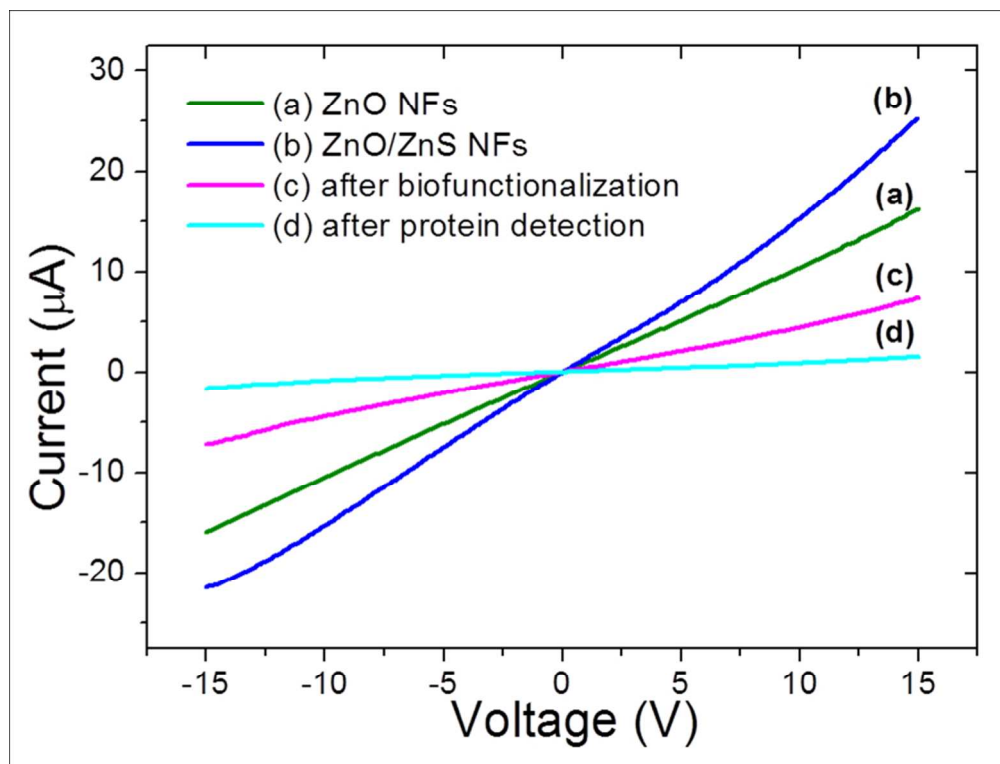


Fig. 10. I-V characteristics of (a) ZnO nanofibers, (b) ZnO nanofibers after sulfidation process - ZnO/ZnS nanofibers (c) ZnO/ZnS nanofibers after binding of tiophene-biotin complex and (d) ZnO/ZnS nanofibers after detection/binding streptavidin labeled with HRP.
153x116mm (150 x 150 DPI)

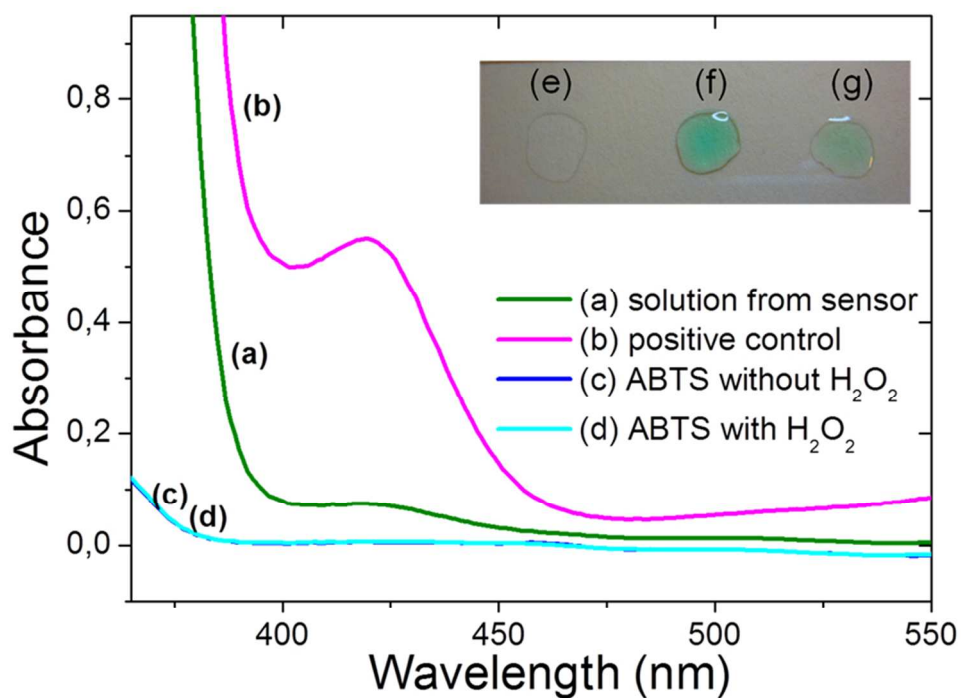


Fig. 11. Absorbance spectra of (a) oxidized ABTS from sensor, (b) oxidized ABTS from control reaction (positive control), (c) reduced ABTS with H₂O₂ (negative control) and (d) reduced ABTS without H₂O₂ (negative control). The image of three drops of different solutions: (e) ABTS with H₂O₂, (f) ABTS from control reaction and (g) ABTS from device. All solutions were prepared in PBS at 5.2 pH.
250x184mm (96 x 96 DPI)